Hyperfine structure and three-channel quantum-defect theory of $6snd\ ^1D_2$ Rydberg states of Ba

H. Rinneberg and J. Neukammer
Institut für Atom- und Festkörperphysik, Freie Universität Berlin, D-1000 Berlin 33, West Germany
(Received 30 June 1982; revised manuscript received 1 September 1982)

The hyperfine structure of $6snd\ ^1D_2$ Rydberg states of ^{135,137}Ba is reported for principal quantum numbers ranging between $n=10$ and $n=50$. From our data, singlet-triplet mixing coefficients have been deduced. A three-channel quantum-defect model has been used to analyze the resonance in singlet-triplet mixing of $6snd\ ^1D_2$ and $^3D_2$ Rydberg states in the vicinity of the $5d7d\ ^1D_2$ perturber. For the determination of the scattering matrix, hyperfine-structure data were found to be essential. Good agreement has been achieved between calculated and experimental singlet-triplet mixing coefficients.

INTRODUCTION

Many aspects of the atomic structure of alkaline-earth elements have been successfully interpreted with the aid of the multichannel quantum-defect theory (MQDT).[1-5] Up to now such analyses of interacting Rydberg series were based upon experimental term values only. Recently, the singlet-triplet mixing of $6snd\ ^1D_2$ Rydberg states of barium, derived from hyperfine-structure measurements,[6] were found to be in sharp disagreement with predictions made by a nine-channel quantum-defect analysis[4] of the even-parity, $J=2$ Ba Rydberg states. This suggests that term values may represent a too limited data set to derive all elements of the $U_{i\alpha}$ scattering matrix and should be augmented by additional experimental data which sensitively depend on the singlet-triplet mixing. In this paper, we include hyperfine-structure (hfs) data in a MQDT analysis for the first time. For this purpose we analyze the $6snd\ ^1D_2$ and $^3D_2$ Rydberg series of barium within a three-channel model. The incorporation of hfs data enables us to determine the relative phases of the $U_{i\alpha}$ scattering matrix elements necessary to calculate the wave functions of the Rydberg states. Furthermore, previous MQDT analyses of alkaline-earth elements[3-5] assumed singlet-triplet mixing of $msnd\ ^1D_2$ and $^3D_2$ states to be caused by configuration interactions only. In contrast, here we show that hfs data allow the additional singlet-triplet mixing, due to spin-orbit interaction itself, to be determined. Using the notation introduced by Lee and Lu[7] to describe channel interactions, within our model the additional singlet-triplet mixing is represented by a nonvanishing angle θ_{12}.

For the three-channel quantum-defect analysis to be found in Sec. IV, singlet-triplet mixing parameters $\Omega(^1D_2)$ of the $6snd\ ^1D_2$ Rydberg states[6] have been used as input data besides experimental term values. The mixing parameters have been derived from the hfs of the $6snd\ ^1D_2$ Rydberg states, thus incorporating the information contained in the hfs into the three-channel analysis. In Sec. II details of the experimental setup are given, used to measure the hfs of the $6snd\ ^1D_2$ Rydberg states. In Sec. III the analysis of the experimental data including the derivation of the singlet-triplet mixing parameters $\Omega(^1D_2)$ is described in detail.

EXPERIMENT

The $6snd\ ^1D_2$ Rydberg states of barium were populated by resonant two-step excitation from the $6s^2\ ^1S_0$ ground state via the $6s6p\ ^1P_1$ intermediate level. Two tunable, stabilized cw dye lasers were employed (see Fig. 1) operating in the Rhodamine 110 and Stilbene 3 spectral regions. Both laser beams counterpropagated through a barium vapor cell heated to about 480 °C. They were aligned to achieve maximum overlap over the length of the vapor cell. For detection purposes spatial separation of the laser beams was necessary outside the resonance cell. This was accomplished by accepting a small crossing angle (see Fig. 1) or by inserting a prism (not shown in Fig. 1) into the laser beams in front of the detector. The first laser was tuned to the resonance line $6s^2\ ^1S_0 \rightarrow 6s6p\ ^1P_1$ ($\lambda_1=533.7$ nm) and kept fixed at an arbitrary position within the Doppler contour. The second laser was scanned across the upper atomic transition $6s6p\ ^1P_1 \rightarrow 6snd\ ^1D_2$ ($\lambda_2=417$–470 nm). Signals were recorded monitoring the transmission of the first

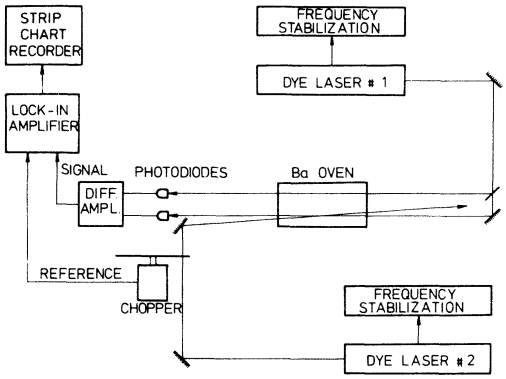

FIG. 1. Experimental setup.

laser beam as a function of the frequency of the second laser. In order to suppress intensity fluctuations of the first laser, the transmission was measured relative to a reference beam. A typical spectrum is shown in Fig. 2. Doppler-free signals were recorded since only those atoms which belong to velocity ensembles being resonant with both laser beams simultaneously are excited to the final state.[8,9] For the first laser beam the resonance cell was optically thick, absorbing about 90% of the incident laser intensity ($\sim$300 μW). This was achieved by adjusting either the temperature of the vapor cell or the detuning of the first laser from the center frequency of the resonance transition. The vapor cell was virtually transparent for the second laser beam with a typical intensity of about 2 mW. Both laser beams were linearly polarized. The angle between both polarization vectors was chosen to obtain optimum signal-to-noise ratios. A marker cavity with a free spectral range of 74.5 MHz provided the necessary frequency calibration.

Contrary to a measurement of the absorption of the second laser beam to monitor the excitation to the barium Rydberg states, the technique described here is very sensitive since it exploits optical pumping effectively. The first laser beam sustains an optical pumping cycle between the ground and intermediate level. During its passage through the laser beams with a diameter of typically 1 mm, an atom can be excited about 100 times since its transit time of several μsec is much longer than the lifetime $\tau=8.4$ nsec of the intermediate $6s\,6p\ ^1P_1$ level. This optical pumping cycle is interrupted when the atom is excited from the intermediate to the final state by absorbing one photon from the second laser beam. This results in a considerably enhanced transmission of the green laser beam provided the atom does not return to the ground or intermediate level within its transit time through the laser beams. This condition is easily fulfilled for Rydberg states because of their long lifetimes and the many possible decay channels to lower-lying levels. Since this enhancement is observed on nearly zero background, an increase in signal-to-noise ratio by a factor of about 50 was achieved compared to the measurement of the absorption of the second laser beam. A quantitative discussion of the optical-optical double-resonance technique employed here is given in Ref. 10.

DATA ANALYSIS

The spectrum (cf. Fig. 2) shows the hfs of the odd isotopes ^{135,137}Ba and the signals corresponding to

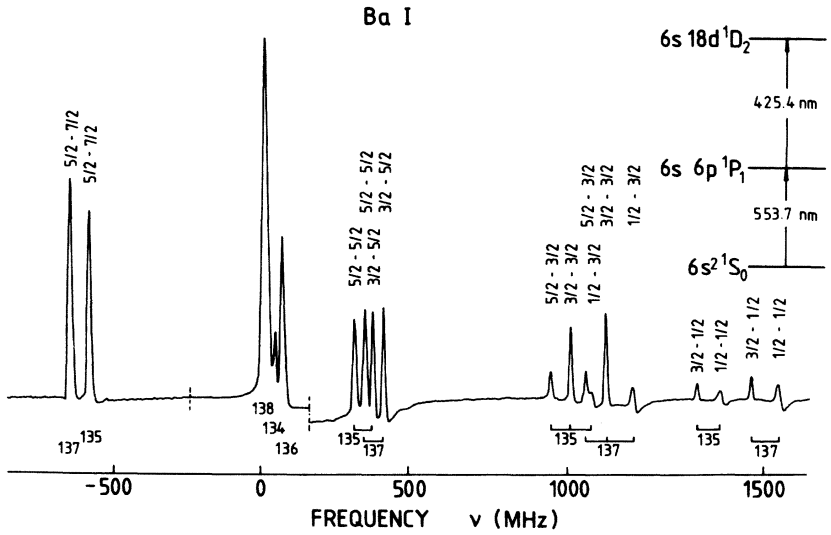

FIG. 2. Doppler-free spectrum of the $6s\,18d\ ^1D_2$ Ba Rydberg state using two-step excitation.

the even ones ^{134,136,138}Ba for the $6s\,18d\,{}^1D_2$ Rydberg state. All frequencies were measured versus ^{138}Ba. The isotope shifts between the even isotopes are clearly resolved. The hyperfine components were labeled F_i-F_f according to the hyperfine levels F_i and F_f of the intermediate and final state involved in the two-step cascade. The frequency separation between the hyperfine component F_i-F_f of the odd isotope A and the signal of ^{138}Ba is denoted as $\delta\Omega_2^{A\text{-}138}(F_i\text{-}F_f)/2\pi$, where

$$\delta\Omega_2^{A\text{-}138}(F_i\text{-}F_f)=\Omega_2^A(F_i\text{-}F_f)-\Omega_2^{138}\ . \tag{1}$$

In this section all transition frequencies or energy splittings represented by a capital Greek letter (e.g., Ω_2^{138}) refer to moving atoms, whereas lower case Greek letters (e.g., ω_2^{138}) apply to atoms at rest. The frequencies Ω_2 appearing on the right-hand side of Eq. (1) correspond to the frequencies of the second laser necessary to excite the atoms from the intermediate to the final state. For the odd isotope A the transition occurs between the hyperfine levels F_i and F_f of the intermediate and final state, respectively. Whereas these transition frequencies depend on the velocity of the atoms and hence on the detuning of the first laser within the Doppler contour, the difference $\delta\Omega_2^{A\text{-}138}(F_i\text{-}F_f)$ is independent of the frequency of the first laser. However, since different velocity ensembles are excited for different isotopes or different hyperfine levels F_i of the intermediate state by the first laser, the frequency separation $\delta\Omega_2^{A\text{-}138}(F_i\text{-}F_f)$ contains contributions originating from the isotope shifts of both transitions as well as the hfs of the intermediate and final state. Since the isotope shifts of the resonance line[11] and the hfs of the intermediate $6s\,6p\,{}^1P_1$ level[11] are well known, their contributions can be quantitatively taken into account. For this purpose we use the following equation:

$$\delta\omega_2^{A\text{-}138}(F_f)=\delta\Omega_2^{A\text{-}138}(F_i\text{-}F_f)-\delta\omega_1^{A\text{-}138}\frac{\omega_2}{\omega_1}$$

$$-\delta\omega_i^A(F_i,\text{c.g.})\frac{\omega_2-\omega_1}{\omega_1}\ , \tag{2}$$

which can be easily derived[8,10] with the aid of a simple hole-burning model. Here

$$\delta\omega_2^{A\text{-}138}(F_f)=\omega_2^A(\text{c.g.-}F_f)-\omega_2^{138} \tag{3}$$

is the difference in frequency for the upper atomic transition between the odd isotope A and ^{138}Ba. For the former isotope the transition frequency ω_2^A (c.g.-F_f) is measured between the center of gravity (c.g.) of the hfs of the intermediate level and the hyperfine component F_f of the final state (see Fig. 3). The second term on the right-hand side of Eq. (2) takes

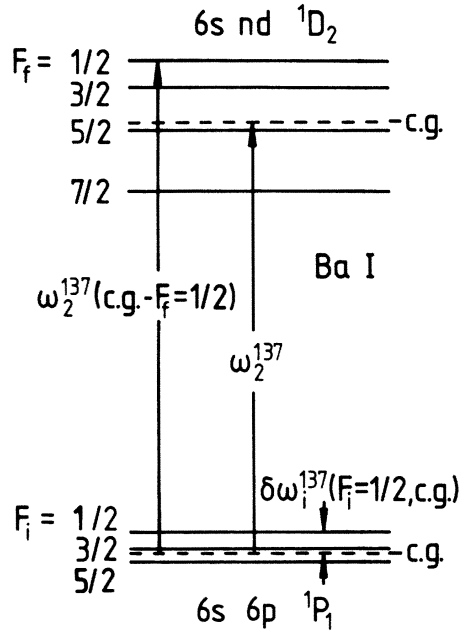

FIG. 3. Illustration of transition frequencies and frequency separations used in Eqs. (2)–(5).

the contribution of the isotope shifts $\delta\omega_1^{A\text{-}138}$ into account, where

$$\delta\omega_1^{A\text{-}138}=\omega_1^A-\omega_1^{138}\ . \tag{4}$$

As can be seen from Eq. (2) the isotope shifts are scaled with the ratio of the transition frequencies of the two-step cascade. The third term corrects for the hyperfine splitting $\delta\omega_i^A(F_i,\text{c.g.})$ (cf. Fig. 3) of the intermediate level. It follows from Eq. (2) that the hfs of the intermediate state appears in the spectra (cf. Fig. 2) reduced by the relative difference in transition frequencies $(\omega_2-\omega_1)/\omega_1$. The isotope shift of the second transition

$$\delta\omega_2^{A\text{-}138}=\omega_2^A-\omega_2^{138} \tag{5}$$

is contained in the frequency separation $\delta\omega_2^{A\text{-}138}(F_f)$.

In Table I we list for both odd isotopes $A=135$, 137 the experimentally observed relative positions of the hyperfine components $\delta\Omega_2^{A\text{-}138}(F_i\text{-}F_f)/2\pi$ for the $6snd\,{}^1D_2$ Rydberg states with principal quantum numbers ranging between $n=10$ and 50. Except for $n=30$, the frequency separations have been measured with an accuracy of ± 15 MHz or better. Since the hfs of the $6s\,30d\,{}^1D_2$ state is comparable to the reduced hfs of the intermediate level, a complicated pattern was observed. In Table I the center of the observed structure is given. Using Eq. (2), the relative positions of the hyperfine components $\delta\Omega_2^{A\text{-}138}(F_i\text{-}F_f)$ have been corrected for the hyperfine splitting of the intermediate state to obtain

TABLE I. Experimentally observed positions of the hyperfine components of ^{135,137}Ba for $6snd\ ^1D_2$ states. Values are given in MHz and are measured versus ^{138}Ba. Accuracy amounts to ±15 MHz or better, except for $n=30$ (±100 MHz).

	$\delta\Omega_2^{137\text{-}138}(F_i\text{-}F_f)/2\pi$							
n	5/2-7/2	5/2-5/2	3/2-5/2	5/2-3/2	3/2-3/2	1/2-3/2	3/2-1/2	1/2-1/2
10	1193			−891	−848	−785	−1361	−1299
11	−463	239	284	742	791	854	1097	1167
12	−173	182	239	437	490	564	645	715
13	−638	275	329	926	981	1058	1373	1448
14	−1131	227	283	1289	1344	1424	2018	2098
15	−594	270	330	890	948	1035	1322	1402
16	−628	276	337	920	981	1066	1370	1453
17	−618	337	397	999	1059	1144	1451	1535
18	−673	339	403	1062	1122	1204	1552	1636
19	−716	392	457	1168	1230	1314	1685	1770
20	−773		484	1243	1309	1389	1808	1888
21	−864	483	541		1467	1550	2005	2085
22	−736	705	766	1638	1697	1769	2209	2290
23	−946	738	799	1815	1879	1961	2495	2577
24	−1048	883	950	2087	2149	2242	2816	2903
25	−821	1174	1238	2378	2443	2534	3102	3193
26	2374	−472	−405	−2330	−2263	−2177	−3313	−3225
27	1185	83	135	−738	−670		−1160	−1065
28	880	219	283	−254	−192	−106	−468	−383
29	640		437		251		146	
30	480	480	480	480	480	480	480	480
31	444	598	664		782	865	856	941
32	421	681	746	887	947	1034	1066	1152
35	498	869	934		1272	1358	1497	1584
50	1673	2075	2139		2371	2459	2497	2584
				$\delta\Omega_2^{135\text{-}138}(F_i\text{-}F_f)/2\pi$				
10	1080			−783	−738	−689	−1201	−1150
11	−404	226	266	671	722	769	991	1046
12	−147	174	227	400	453	509	589	646
13	−562	256	308	837	890	950	1242	1300
14	−982	227	283	1175	1228		1824	1883
15	−526	249	308	804	858	923	1193	1260
16	−556	253	312	827	888		1233	1302
17	−553	300	360	895	954	1018	1307	1372
18	−602	304	366	950	1012	1081	1395	1462
19	−643	347	412	1042	1106		1514	1580
20	−694	373	433	1114	1176	1243	1618	1685
21	−778	417	483	1260	1323	1391	1809	1875
22	−688	603	668	1452	1511	1578	1978	2050
23	−883	638	696	1619	1677	1741	2241	2307
24	−985	753	815	1862	1921	1991	2532	2599
25	−821	1002	1063	2121	2178	2249	2791	2860
26	2147	−389	−324	−2057	−1990	−1920	−2944	−2872
27	1068	83	135		−588	−517	−1023	−957
28	782	186	249	−237	−177	−106	−426	−355
29	555	312	377		211		117	191
30	480	480	480	480	480	480	480	480
31	360	501	566		675	747	741	810
32	333	570	634		819	887	931	999
35	386	731	793		1105		1310	1376
50	1404	1790	1857	2016	2085		2209	2281

$$[\delta\omega_2^{A\text{-}138}(F_f)+\delta\omega_1^{A\text{-}138}\omega_2/\omega_1]/2\pi \ .$$

This quantity has been plotted for ^{137}Ba versus the principal quantum number n in Fig. 4. The contribution of the isotope shift of the first transition causes a vertical displacement virtually independent of n. Figure 4 is identical with Fig. 1(a) of Ref. 6 except for the data points at $n=26$. The $6s\,26d\ ^1D_2$ and $^3D_2$ states of barium, occurring at $E=41\,829.487$ and $41\,831.906$ cm^{-1}, are strongly mixed owing to the interaction with the close-lying $5d\,7d\ ^1D_2$ perturber. Our three-channel QDT described in Sec. IV predicts the lower-lying level to be a $^1D_2$ state in agreement with the notation of Rubbmark *et al.*[12] This identification is supported by recent g-factor measurements.[13] Therefore the data points appearing in Fig. 4 at $n=26$ were derived from the hfs of the level at $E=41\,829.487$ cm^{-1}. In contrast, the reverse designation was concluded from the nine-channel quantum-defect analysis.[4] In Ref. 6, following the designation suggested by the nine-channel QDT analysis, for $n=26$ the hfs shown in Fig. 1 corresponds to the upper state at $E=41\,831.906$ cm^{-1}.

In Table II we list the effective relative positions of the hyperfine components

$$\delta\omega_2^{A\text{-}138}(F_f)/2\pi-\delta\nu_2^{A\text{-}138}(\mathrm{NMS}) \ ,$$

corrected not only for the hfs of the intermediate state but also for the isotope shift of the first as well as the normal mass shift (NMS) of the second transition. The latter contribution is given by

$$\delta\nu_2^{A\text{-}138}(\mathrm{NMS})=\nu_2(A\text{-}138)/(A\times 138\times 1836) \ .$$

Except for $n=30$, the frequencies given in Table II are accurate to ± 15 MHz or better. The last column contains the c.g. of the hfs of the $6snd\ ^1D_2$ Rydberg states relative to ^{138}Ba. Recently, the hfs of $6snd\ ^1D_2$ Rydberg states of Ba has been reported[14] for $n=13$–17, 20, 24. Within experimental error, these measurements are in agreement with our data given for these states in Table II.

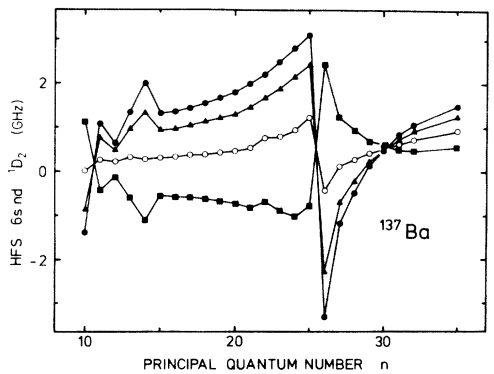

FIG. 4. Hyperfine splitting of the $6snd\ ^1D_2$ series of ^{137}Ba as a function of n. Dots, triangles, circles, and squares correspond to the $F_f=1/2$, 3/2, 5/2, and 7/2 components, respectively.

In the remaining part of this section we derive the singlet-triplet mixing parameters $\Omega(^1D_2)$ from the data given in columns 2–5 of Table II. For this purpose we express the wave function of the $6snd\ ^1D_2$ Rydberg states as

$$\begin{aligned}|\,6snd\ ^1D_2\rangle=&\Lambda(^1D_2)\,|\,6snd\ ^1D_2\rangle_{SL}\\&+\Omega(^1D_2)\,|\,6snd\ ^3D_2\rangle_{SL}\\&+\epsilon(^1D_2)\,|\,5d7d\,J=2\rangle_{SL}\end{aligned}\qquad(6)$$

with $|\epsilon|=(1-\Lambda^2-\Omega^2)^{1/2}$. In Eq. (6), which applies to the even barium isotopes only, the wave function $|\,6snd\ ^1D_2\rangle$ has been expanded in terms of the pure configuration, exactly SL-coupled state vectors $|\,6snd\ ^1D_2\rangle_{SL}$ and $|\,6snd\ ^3D_2\rangle_{SL}$ corresponding to the intermediate basis $|\,\bar{\alpha}\rangle$ conventionally used in MQDT analyses. The last term in Eq. (6) takes the admixture of the doubly excited configuration $5d\,7d$ into the $6snd\ ^1D_2$ Rydberg states into account. It is well known from MQDT[4] that strong admixtures of the $|\,5d7d\ ^1D_2\rangle_{SL}$, $|\,5d7d\ ^3D_2\rangle_{SL}$, $|\,5d7d\ ^3F_2\rangle_{SL}$, and $|\,5d7d\ ^3P_2\rangle_{SL}$ perturbing configuration into the $6snd\ ^1D_2$ Rydberg states occur at $n=14$ and $n=26$. However, since neither the hfs of the $6snd\ ^1D_2$ Rydberg states, nor the isotope shifts of the (second) transition to these states depend on the composition of the admixed perturber fraction in terms of the fine-structure components $|\,5d7d\ ^1D_2\rangle_{SL}$, $|\,5d7d\ ^3D_2\rangle_{SL}$, $|\,5d7d\ ^3F_2\rangle_{SL}$, and $|\,5d7d\ ^3P_2\rangle_{SL}$, in Eq. (6) these perturbing state vectors have been lumped into the last term. Furthermore, because of the small core polarization of the $5d\,7d$ configuration, within our accuracy the last term in Eq. (6) does not contribute to the measured hyperfine splittings of the Rydberg states directly. From the hfs of perturber states belonging to the $5d\,7d$ configuration we estimate the hyperfine interaction of a pure $5d\,7d$ state to be of the order of 1% of that of a $6s$ electron in Ba^+. However, the admixture of the perturbing configuration influences the hfs indirectly by reducing the total $6snd$ character, i.e.,

$$\Omega^2(^1D_2)+\Lambda^2(^1D_2)<1$$

and by changing the singlet-triplet mixing.

For the odd isotopes the strong hyperfine interaction of the $6s$ electron with the nuclear spin may modify the wave functions of the $6snd\ ^1D_2$ states appreciably by coupling the $|\,6snd\ ^1D_2\rangle$ vector to the triplet states $|\,6snd\ ^3D_{1,2,3}\rangle$. The hyperfine-induced

TABLE II. Effective positions of the hyperfine components of ^{135,137}Ba for $6snd\ ^1D_2$ states. Values are given in MHz and are measured versus ^{138}Ba. The accuracy typically amounts to ±15 MHz or better, except for $n=30$ (±100 MHz). In the last column the c.g. is given.

	$\delta\omega_2^{137\text{-}138}(F_f)/2\pi-\delta\nu_2^{137\text{-}138}$ (NMS)				
n	7/2	5/2	3/2	1/2	c.g.
10	984		−1101	−1615	
11	−674	25	529	836	−73
12	−384	−28	226	379	−79
13	−850	61	713	1104	−69
14	−1344	13	1075	1748	−144
15	−807	56	677	1048	−66
16	−841	62	707	1095	−67
17	−832	122	784	1175	−22
18	−887	125	845	1274	−21
19	−930	179	953	1407	13
20	−987	205	1028	1526	25
21	−1078	265	1186	1723	58
22	−951	488	1418	1926	242
23	−1160	521	1599	2219	234
24	−1263	668	1871	2534	323
25	−1035	959	2164	2823	589
26	2160	−686	−2544	−3593	−210
27	971	−152	−951	−1437	9
28	666	4	−471	−751	98
29	426	155	−31	−136	197
30	217	217	217	217	217
31	230	383	497	572	364
32	207	464	664	782	433
35	283	652	987	1213	628
50	1458	1858	2087	2212	1779
	$\delta\omega_2^{135\text{-}138}(F_f)/2\pi-\delta\nu_2^{135\text{-}138}$ (NMS)				
10	854		−1009	−1472	
11	−635	−10	439	711	−98
12	−379	−58	168	304	−105
13	−795	21	603	952	−96
14	−1216	−8	939	1531	−148
15	−761	14	567	901	−97
16	−787	17	592	940	−97
17	−789	64	658	1010	−64
18	−838	68	715	1098	−62
19	−879	113	807	1215	−35
20	−930	135	877	1319	−24
21	−1015	181	1023	1508	4
22	−925	365	1213	1679	150
23	−1119	399	1379	1939	142
24	−1222	515	1622	2229	213
25	−1058	763	1880	2490	431
26	1911	−625	−2292	−3245	−206
27	831	−177	−889	−1327	−31
28	545	−52	−476	−728	34
29	318	75	−91	−183	113
30	199	199	199	199	199
31	123	263	373	437	246
32	96	332	516	627	304
35	149	502	802	1004	471
50	1166	1552	1781	1905	1479

changes of the $|6snd\,^1D_2\rangle$ wave function are pronounced when the energy separations between the $^1D_2$ state and the ^3D configuration are of the same order or even smaller than the hyperfine coupling constant a_{6s} of the 6s electron. On the contrary, for sufficiently large singlet-triplet splittings the wave function [cf. Eq. (6)] of the even isotopes may be used to calculate the hyperfine splitting of the $6snd\,^1D_2$ Rydberg states. Within our experimental accuracy the hyperfine interaction of the outer Rydberg electron with the nuclear spin can be neglected for $n \geq 10$. Hence the Hamiltonian representing the hyperfine interaction can be written as

$$H_{\rm hf}=a_{6s}\vec{s}_1\cdot\vec{I}=a_{6s}\vec{S}\cdot\vec{I}/2+a_{6s}\vec{\sigma}\cdot\vec{I}/2\ , \qquad (7)$$

where $\vec{S}=\vec{s}_1+\vec{s}_2$ and $\vec{\sigma}=\vec{s}_1-\vec{s}_2$. The spin angular momenta $\vec{s}_1$ and $\vec{s}_2$ refer to the 6s electron and Rydberg electron, respectively. For the hyperfine splitting constant a_{6s} the free-ion value $^{137}a_{6s}=4.016$ GHz can be used to a good approximation. Evaluating the matrix element $\langle 6snd\,^1D_2,I,F_f\,|\,H_{\rm hf}\,|\,6snd\,^1D_2,I,F_f\rangle$, the hfs of the $6snd\,^1D_2$ Rydberg state is found to be represented by a hyperfine splitting constant

$$A(^1D_2)=a_{6s}[\Omega^2(^1D_2) -2\sqrt{6}\Lambda(^1D_2)\Omega(^1D_2)]/12\ . \qquad (8)$$

The first term within the square brackets represents the amount of triplet character [cf. Eq. (6)] and stems from the first term of Eq. (7). The interference term [cf. Eq. (8)] is related to the term $a_{6s}\vec{\sigma}\cdot\vec{I}/2$ in Eq. (7). It can be seen from Eq. (8) and was discussed in Ref. 6 that the experimentally determined sign of the hyperfine splitting factor allows the relative sign of the admixture coefficients $\Lambda(^1D_2)$ and $\Omega(^1D_2)$ to be inferred. The admixture coefficients can be deduced separately from Eq. (8) provided the corresponding $6snd\,^1D_2$ state is unperturbed, i.e., $\epsilon=0$. For perturbed states additional information, such as the total perturber character $\epsilon^2=1-\Lambda^2-\Omega^2$, is needed. This quantity can be inferred from a MQDT analysis of term values, lifetime and isotope shift measurements. If the hyperfine-induced modifications of the $|6snd\,^1D_2\rangle$ wave function of the odd Ba isotopes cannot be neglected, the positions of the hyperfine components are shifted in such a way that an exact description of the hfs by a splitting constant A might not be possible any more. Therefore we have calculated for each value of the principal quantum number n the effective relative positions of the hyperfine components by diagonalizing the Hamiltonian $H=H_0+H_{\rm hf}$. Here H_0 represents the Hamiltonian of the barium isotopes apart from hyperfine effects. The Hamiltonian is set up, using the state vector given in Eq. (6) and the following wave functions of the $6snd\,^3D$ states as basis,

$$\begin{aligned}
|6snd\,^3D_1\rangle&=\Lambda(^3D_1)\,|\,6snd\,^3D_1\rangle_{SL}+\epsilon(^3D_1)\,|\,5d\,7d\,J=1\rangle_{SL}\ ,\\
|6snd\,^3D_2\rangle&=\Omega(^3D_2)\,|\,6snd\,^1D_2\rangle_{SL}+\Lambda(^3D_2)\,|\,6snd\,^3D_2\rangle_{SL}+\epsilon(^3D_2)\,|\,5d\,7d\,J=2\rangle_{SL}\ ,\\
|6snd\,^3D_3\rangle&=\Lambda(^3D_3)\,|\,6snd\,^3D_3\rangle_{SL}+\epsilon(^3D_3)\,|\,5d\,7d\,J=3\rangle_{SL}\ .
\end{aligned} \qquad (9)$$

For the even isotopes $H=H_0$ is diagonal with experimental term values appearing as diagonal elements. The term values of the $6snd$ Rydberg series were taken from Refs. 12, 15, and 16. In order to calculate the matrix elements of $H_{\rm hf}$ [cf. Eq. (7)] the angular part $|J,I,F_f\rangle$ was included into the state vectors in Eqs. (6) and (9). Since F_f is a rigorous quantum number, the Hamiltonian was set up for each F_f value separately. Matrix elements of $H_{\rm hf}$ were calculated using standard angular momentum algebra. Some of these matrix elements can be found in Ref. 17. After diagonalization isotope shifts were added to the calculated eigenvalues for comparison with the experimental results listed in columns 2–5 of Table II. Within a least-squares fit procedure the hfs of both odd isotopes ^{135,137}Ba was calculated simultaneously. For $11 \leq n \leq 27$ the measured hfs of the $^3D_2$ and some $^3D_1$ states was included in the fit. The hfs of the ^{3}D states[18] sensitively depends on the splittings between the triplet states and the composition of their wave functions. On the contrary, these quantities play a lesser role for the hfs of the $6snd\,^1D_2$ states. Therefore in the present analysis $\Omega(^1D_2)$ is the essential fitting parameter. In Table III the singlet-triplet mixing parameters $\Omega(^1D_2)$ obtained from the least-squares fit have been listed. The absolute phases of the wave functions [cf. Eqs. (6) and (9)] were chosen arbitrarily in such a way that the largest admixture coefficients (Λ) are positive. The somewhat larger error limits for states above $n=23$ are due to the uncertain positions of the $^3D_3$ states. The value given for $\Omega(^1D_2)$ at $n=30$ represents a conservative estimate using $A(n=30)=0(25)$ MHz. In Fig. 5 we have

plotted the singlet-triplet mixing parameter $\Omega(^1D_2)$ (cf. Table III) versus the principal quantum number n.

DISCUSSION

Although the influence of the local perturber $5d7d\,^3F_2$ at $n=14$ is clearly visible, the prominent feature of Fig. 5 is the dispersionlike resonance occurring in the vicinity of the $5d7d\,^1D_2$ perturber around $n=26$. This resonance has been reported and discussed previously.[6] Although a nine-channel quantum-defect analysis has been carried out before to describe all bound, even-parity, $J=2$ states with term values above 30237 cm^{-1},[4] for the sake of transparency we restrict ourselves to a three-channel QDT to examine this resonance within the limited energy interval $20 \leq n \leq 35$. Previously,[19] this model was successfully used to explain the total perturber fraction of the $6snd\,^1D_2$ and $^3D_2$ Rydberg states close to the $5d7d\,^1D_2$ perturber. Using the standard notation, the channels and relevant parameters are listed in Table IV. Naturally, our model cannot account for the fine structure of the $5d7d$ configuration. Therefore we assume the $5d7d\,^1D_2$ state to be a member of a series converging versus either the $^2D_{3/2}$ or $^2D_{5/2}$ state of Ba^+. This is equivalent to assuming pure jj coupling for the perturber component of the $5d7d\,^1D_2$ vector. Although this is only approximately true, it is well known from MQDT analyses of odd-[5] and even-[4] parity states of barium that doubly excited configurations $5dnl$ ($l=2,3$) are best described by jj coupling.

TABLE III. Singlet-triplet mixing parameters Ω of $6snd\,^1D_2$ Rydberg states of Ba with term values listed in the first column. Mixing amplitudes $\Omega(^1D_2)$ are derived from the data listed in Table II. Error limits include uncertainties caused by the data analysis.

n	E_n (cm^{-1})[a]	$\Omega(^1D_2)$
10	39998.339	−0.20(5)
11	40483.579	0.13(3)
12	40781.420	0.07(3)
13	41007.712	0.17(3)
14	41162.415	0.36(5)
15	41315.547	0.16(2)
16	41417.641	0.17(2)
17	41500.067	0.18(2)
18	41567.184	0.19(2)
19	41622.465	0.21(2)
20	41668.528	0.23(2)
21	41707.296	0.26(2)
22	41740.182	0.29(2)
23	41768.349	0.35(2)
24	41792.623	0.44(4)
25	41813.571	0.55(4)
26	41829.487	−0.53(4)
27	41852.055	−0.24(4)
28	41864.689	−0.12(4)
29	41877.007	−0.05(4)
30	41888.108	0.00(4)
31	41898.206	0.03(4)
32	41907.371	0.06(4)
35	41929.828	0.09(4)
50	41985.979	0.20(4)

[a]References 12 and 16.

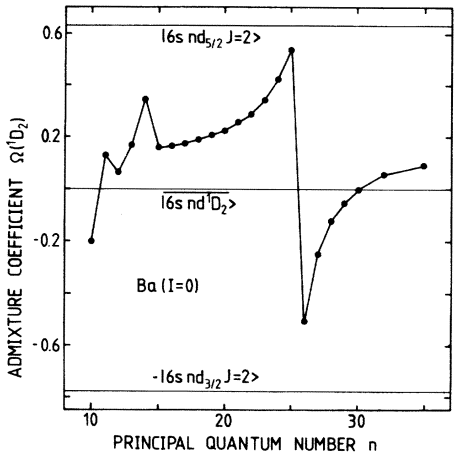

FIG. 5. Singlet-triplet mixing coefficient $\Omega(^1D_2)$ derived from the data listed in Table II. In Fig. 5 the exactly SL-coupled basic vector is denoted by a horizontal bar.

In the following paragraph we outline the analysis and list the pertinent equations. For a thorough discussion of MQDT the reader is referred to Refs. 1, 2, 7, 20, and 21. For each term value E_n, a set of three effective quantum numbers $\nu_i^{(n)}$ is defined according to the following equation:

$$E_n = I_i - R/(\nu_i^{(n)})^2 \quad (i=1,2,3) \tag{10}$$

where $I_1=I_2=I_s$, $I_3=I_d$ denotes the corresponding ionization energies and $\nu_1^{(n)}=\nu_2^{(n)}=\nu_s^{(n)}, \nu_3^{(n)}=\nu_d^{(n)}$, and R stands for the mass-corrected Rydberg constant. For the Rydberg states, the boundary condition of the wave function at $r\rightarrow\infty$ leads to the following equation:

$$\sum_{\alpha=1}^{3} A_\alpha F_{i\alpha} = \sum_{\alpha=1}^{3} A_\alpha U_{i\alpha} \sin[\pi(\nu_i+\mu_\alpha)] = 0 \,. \tag{11}$$

Here A_α are the expansion coefficients of the wave function of the Rydberg states in terms of the wave functions of the close-coupling channels with corresponding eigenquantum defects μ_α.[1,2,7,20,21] The (nontrivial) solution

TABLE IV. Results of the three-channel QDT analysis.

$i,\alpha,\bar{\alpha}$	1	2	3
$\|i\rangle$	$6snd_{5/2}$	$6snd_{3/2}$	$5d7d$
$\|\bar{\alpha}\rangle$	$6snd\,^1D_2$	$6snd\,^3D_2$	$5d7d$
$U_{i\bar{\alpha}}$	$(3/5)^{1/2}$	$(2/5)^{1/2}$	0
	$-(2/5)^{1/2}$	$(3/5)^{1/2}$	0
	0	0	1
I_i	42035.02	42035.02	46908.89[a]
(cm^{-1})			47709.86[b]
μ_i	0.694[a]	0.784[a]	0.345[a]
	0.708[b]	0.786[b]	0.658[b]
θ_{ij}	$\theta_{12}=0.193$[a]	$\theta_{13}=\pm0.091$[a]	$\theta_{23}=\mp0.054$[a]
	0.314[b]	±0.576[b]	∓0.172[b]

[a] $I_d={}^2D_{3/2}(Ba^+)$.
[b] $I_d={}^2D_{5/2}(Ba^+)$.

$$A_\alpha=C_{i\alpha}\Big/\left[\sum_{\alpha=1}^{3}C_{i\alpha}^2\right]^{1/2} \tag{12}$$

of Eq. (11) requires the determinant $|F_{i\alpha}|$ to vanish. In Eq. (12), i may be taken arbitrarily ($i=1$–3) and $C_{i\alpha}$ is the corresponding cofactor of the determinant $|F_{i\alpha}|$. Using $\det F_{i\alpha}=0$, ν_s can be written in terms of ν_d according to the following expression:

$$\nu_{s_{1,2}}=\nu_d+(1/\pi)\cot^{-1}\{-(M_{11}+M_{22})/2\pm[(M_{11}-M_{22})^2/4+M_{12}^2]^{1/2}\}\ , \tag{13}$$

where M_{ij} is defined[21] as

$$M_{ij}=\sum_{\alpha=1}^{3}U_{i\alpha}U_{j\alpha}\cot[\pi(\nu_d+\mu_\alpha)]\ . \tag{14}$$

Figure 6 shows the usual Lu-Fano plot,[1] where both solutions ν_{s_1},ν_{s_2} are plotted modulo 1 vs ν_d. Solutions (ν_{s_1},ν_d) and (ν_{s_2},ν_d) of Eq. (13), simultaneously satisfying Eq. (10), correspond to theoretical term values. From experimental term values, ν_s(exp) and ν_d(exp) were calculated according to Eq. (10). In Fig. 6 open circles and squares correspond to experimental energies of the $6snd\,^1D_2$ and $^3D_2$ states, respectively.

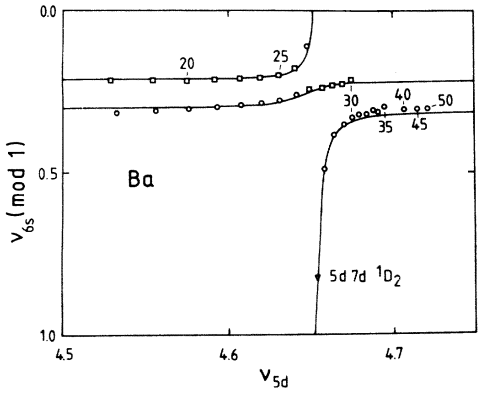

FIG. 6. Lu-Fano plot calculated using the parameters given in Table IV with $6snd\,^1D_2$ (○), $6snd\,^3D_2$ (□), and $5d7d\,^1D_2$ (▽), representing experimental data.

Apart from term values, MQDT allows us to calculate the wave functions of the Rydberg states. Choosing the collision channels $|i\rangle$ (cf. Table IV) as basis, the expansion coefficients are given[2,7] by

$$Z_i^{(n)}=(-1)^{l_i+1}(\nu_i^{(n)})^{3/2}\times\sum_{\alpha=1}^{3}U_{i\alpha}\cos[\pi(\nu_i^{(n)}+\mu_\alpha)]A_\alpha^{(n)}/N_n\ , \tag{15}$$

where the normalization factor N_n is reported in Eq. (2.7) of Ref. 7. Since the $6snd$ Rydberg states are predominantly SL coupled, it is preferable to use the exactly SL-coupled intermediate basis $|\bar{\alpha}\rangle$ (cf. Table IV). The expansion coefficients $Z_i^{(n)}$ are converted to amplitudes $Z_{\bar{\alpha}}^{(n)}$ by means of the (jj-SL) recoupling matrix $U_{i\bar{\alpha}}$ (cf. Table IV)

$$Z_{\bar{\alpha}}^{(n)}=\sum_{i=1}^{3}Z_i^{(n)}U_{i\bar{\alpha}}\ . \tag{16}$$

It should be noted that the expansion coefficients $Z_{\bar{\alpha}=1}(6snd\,^1D_2)$, $Z_{\bar{\alpha}=2}(6snd\,^1D_2)$, and $Z_{\bar{\alpha}=3}(6snd\,^1D_2)$ were labeled $\Lambda(^1D_2)$, $\Omega(^1D_2)$, and $\epsilon(^1D_2)$, respectively, in the preceding section and in

Ref. 6. For the MQDT analysis the same definition of the absolute phases of the wave functions was used as discussed above. Following Lee and Lu,[7] the $U_{i\alpha}$ scattering matrix is decomposed into the recoupling matrix $U_{i\bar{\alpha}}$ and the matrix $V_{\bar{\alpha}\alpha}$ which describes the channel interactions and is generated by three successive rotations through generalized Eulerian angles θ_{12}, θ_{13}, and θ_{23}. Within a least-squares fit procedure experimental energies E_n and singlet-triplet mixing parameters $\Omega_n(^1D_2)$ were compared with theoretical values for $20 \leq n \leq 35$. Although the eigenquantum defects μ_α ($\alpha=1,2,3$) were adjusted, too, the essential free parameters are the three angles θ_{ij}.

The ionization limit I_s of the $6snd$ series is well known and was taken from Ref. 4. Consequently, the eigenquantum defects μ_1 and μ_2 are essentially fixed. The choice of the ionization limit for the $5dnd$ series detemines μ_3. Because of the limited energy range under consideration, all parameters were taken to be independent of energy, i.e., independent of n. Choosing the $^2D_{3/2}$ state of Ba^+ as series limit for the $5dnd$ perturbing channel, the results of the least-squares fit procedure are listed in Table IV. Good agreement was achieved for term values and the corresponding wave functions, as can be seen from the Lu-Fano plot (cf. Fig. 6) and the resonance of the singlet-triplet mixing parameter $\Omega(^1D_2)$ shown in Fig. 7(a). As mentioned above, our three-channel analysis can be carried out, alternatively assuming the $5dnd$ series to converge versus the $^2D_{5/2}$ limit at $I_d=47\,709.86$ cm^{-1}. Within our model both sets of parameters are equivalent and describe the same physical situation. As a matter of fact, varying the assumed ionization limit I_d between the two limits $^2D_{3/2}$ and $^2D_{5/2}$, both sets of parameters can be transformed continuously into each other. It is interesting to note that the angle θ_{12} never vanishes, but always stays positive. The sign of θ_{12} is determined by our phase convention given above. For the following discussion of the singlet-triplet mixing resonance we assume $I_d=46\,908.89$ cm^{-1} ($^2D_{3/2}$).

Whereas good agreement between experimental and calculated singlet-triplet mixing parameters is achieved [cf. Fig. 7(a)] when θ_{12} is different from zero ($\theta_{12}=0.193$), setting $\theta_{12}=0$ and leaving all remaining parameters of Table IV unchanged produces an offset between experimental and theoretical values for $\Omega(^1D_2)$, as can be seen from Fig. 7(b). Since θ_{12} describes essentially the interaction between the $6snd\,^1D_2$ and $6snd\,^3D_2$ channels, the offset is interpreted as that part of the singlet-triplet mixing which is produced by the spin-orbit interaction itself, even in the absence of any configuration interactions. In addition, the configuration interaction with the $5d7d\,^1D_2$ perturbing state causes the Fano-like resonance which is superimposed on the constant contribution of the singlet-triplet mixing due to the spin-orbit interaction. The shift in the position of the calculated resonance, seen in Fig. 7(b), is simply caused by the change in the character of the state at $n=26$ when θ_{12} is set equal to zero. In Figs. 7(b) and 7(c) the calculated value $\Omega(n=26)$ actually corresponds to a triplet state. Furthermore, it is important to know that Figs. 7(a)–7(c) correspond to identical Lu-Fano plots (cf. Fig. 6). Hence θ_{12} cannot be deduced from term values only in a MQDT analysis.

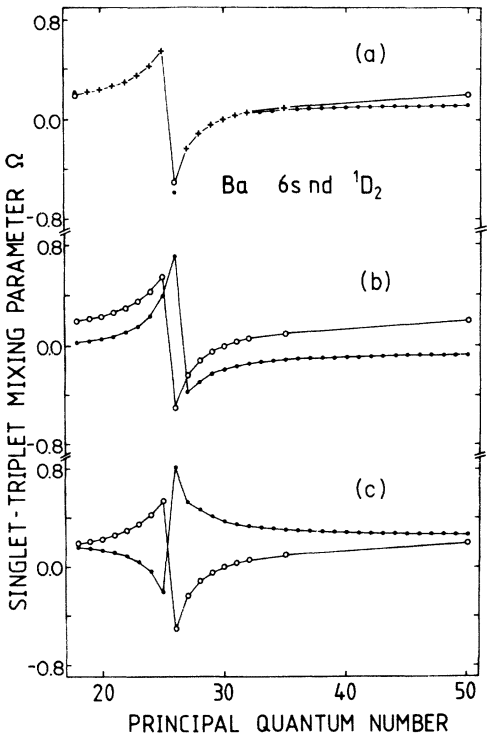

FIG. 7. Experimental (○) and calculated (●) singlet-triplet mixing parameters $\Omega(n)$; (+) indicates agreement within experimental accuracy. (a) Calculated values were obtained using the parameters given in Table IV; (b) θ_{12} was set equal to zero; (c) the relative sign of θ_{13} and θ_{23} was changed.

Calculated values for the singlet-triplet mixing parameter, shown in Fig. 7(c), were obtained by changing the relative sign of θ_{13} and θ_{23}. Whereas the Lu-Fano plot is not affected at all, strong disagreement is observed between experimental and theoretical singlet-triplet mixing parameters Ω. It follows that the relative sign of θ_{13} and θ_{23} can be deduced immediately from hfs measurements.

In summary, by including hfs data in a MQDT analysis we have shown that term values are insuffi-

cient to determine the $U_{i\alpha}$ scattering matrix unambiguously, at least for Rydberg series converging versus the same ionization limit. Although a simple three-channel model was used, the same physical conclusions were derived from a four-channel analysis which included the fine-structure component $^3F_2$ of the $5d\,7d$ perturbing configuration.

ACKNOWLEDGMENTS

This work was supported by the Deutsche Forschungsgemeinschaft, Sonderforschungsbereich 161. The continuous support and interest of Professor E. Matthias is acknowledged. We thank Dr. P. Camus for communicating term values to us prior to publication.

[1]J. J. Wynne and J. A. Armstrong, Comments At. Mol. Phys. 8, 155 (1979) and references therein.
[2]J. A. Armstrong, P. Esherick, and J. J. Wynne, Phys. Rev. A 15, 180 (1977).
[3]P. Esherick, Phys. Rev. A 15, 1920 (1977).
[4]M. Aymar and O. Robaux, J. Phys. B 12, 531 (1979).
[5]J. A. Armstrong, J. J. Wynne, and P. Esherick, J. Opt. Soc. Am. 69, 211 (1979).
[6]H. Rinneberg and J. Neukammer, Phys. Rev. Lett. 49, 124 (1982).
[7]C. M. Lee and K. T. Lu, Phys. Rev. A 8, 1241 (1973).
[8]C. Delsart and J.-C. Keller, Opt. Commun. 15, 91 (1975).
[9]J. E. Bjorkholm and P. F. Liao, Phys. Rev. A 14, 751 (1976).
[10]J. Neukammer and H. Rinneberg, J. Phys. B 15, 2899 (1982).
[11]G. Nowicki, K. Bekk, S. Göring, A. Hanser, H. Rebel, and G. Schatz, Phys. Rev. C 18, 2369 (1978).
[12]J. R. Rubbmark, S. A. Borgström, and K. Bockasten, J. Phys. B 10, 421 (1977).
[13]K. Bhatia, P. Grafström, C. Levinson, H. Lundberg, L. Nilsson, and S. Svanberg, Z. Phys. A303, 1 (1981).
[14]P. Grafström, J. Zhan-Kui, G. Jönsson, S. Kröll, C. Levinson, H. Lundberg, and S. Svanberg, Z. Phys. A306, 281 (1982).
[15]P. Camus, M. Dieulin, and A. El Himdy, Phys. Rev. A 26, 379 (1982).
[16]M. Aymar, P. Camus, M. Dieulin, and C. Morillon, Phys. Rev. A 18, 2173 (1978).
[17]J. Neukammer and H. Rinneberg, J. Phys. B 15, 3787 (1982).
[18]J. Neukammer and H. Rinneberg, J. Phys. B 15, L723 (1982).
[19]T. F. Gallagher, W. Sandner, and K. A. Safinya, Phys. Rev. A 23, 2969 (1981).
[20]U. Fano, J. Opt. Soc. Am. 65, 979 (1975).
[21]K. T. Lu, Phys. Rev. A 4, 579 (1971).